JOURNAL OF GEOPHYSICAL RESEARCH, VOL. 114, C03020, doi:10.1029/2007JC004646, 2009

Neural network-based estimates of North Atlantic surface pCO_2 from satellite data: A methodological study

T. Friedrich[1,2] and A. Oschlies[1]

Received 14 November 2007; revised 23 September 2008; accepted 12 January 2009; published 26 March 2009.

[1] A new method is proposed to estimate ocean surface pCO_2 from remotely sensed surface temperature and chlorophyll data. The method is applied to synthetic observations provided by an eddy-resolving biogeochemical model of the North Atlantic. The same model also provides a perfectly known simulated pCO_2 ''ground truth'' used to quantitatively assess the success of the estimation method. Model output is first sampled according to realistic voluntary observing ship (VOS) and satellite coverage. The model-generated VOS ''observations'' are then used to train a self-organizing neural network that is subsequently applied to model-generated ''satellite data'' of surface temperature and surface chlorophyll in order to derive basin-wide monthly maps of surface pCO_2. The accuracy of the estimated pCO_2 maps is analyzed with respect to the ''true'' surface pCO_2 fields simulated by the biogeochemical circulation model. We also investigate the accuracy of the estimated pCO_2 maps as a function of VOS line coverage, remote sensing errors, and the interpolation of missing remote sensing data due to cloud cover and low solar irradiation in winter. For a simulated ''sampling'' corresponding to VOS lines and patterns of optical satellite coverage of the year 2005, the neural net can successfully reproduce pCO_2 from model-generated ''remote sensing data'' of SST and Chl. Basin-wide RMS errors amount to 19.0 μatm for a hypothetical perfect interpolation scheme for remote sensing data gaps and 21.1 μatm when climatological surface temperature and chlorophyll values are used to fill in areas lacking optical satellite coverage.

Citation: Friedrich, T., and A. Oschlies (2009), Neural network-based estimates of North Atlantic surface pCO_2 from satellite data: A methodological study, *J. Geophys. Res.*, *114*, C03020, doi:10.1029/2007JC004646.

1. Introduction

[2] With respect to the Earth's radiation balance, CO_2 is the most important anthropogenically affected greenhouse gas, whose content in the atmosphere has increased by 30% since the beginning of the industrial revolution. Still, the atmospheric increase constitutes only about half of the accumulated anthropogenic emissions. The ocean is thought to have absorbed some 40% of these emissions so far [*Sabine et al.*, 2004]. However, estimates of regional patterns and temporal fluctuations of the ocean's CO_2 uptake are prone to large uncertainties. Reducing the uncertainties in air-sea CO_2 fluxes on synoptic scales is also relevant for improved estimates of regional terrestrial carbon sources and sinks, which eventually have to be accounted for in suitable schemes to monitor and control anthropogenic CO_2 emissions.

[3] A direct calculation of the air-to-sea CO_2 flux requires detailed knowledge of the gas transfer velocity and the partial pressure of CO_2 (pCO_2) in the ocean's surface waters. In the Atlantic Ocean a pCO_2 monitoring network was initialized by the European project CAVASSOO (Carbon Variability Studies by Ships of Opportunity) in 2001. It is currently extended with better coverage and higher measurement accuracy by the European CARBOOCEAN project in cooperation with US/American partners (Table 1).

[4] In contrast to CO_2 concentrations in the well mixed atmosphere, seawater pCO_2 is subject to high spatial and temporal variability at the ocean's surface as a result of changes in solubility, mainly driven by temperature. Furthermore, marine biology alters the total dissolved inorganic carbon (DIC) content of the water which affects pCO_2. Voluntary observing ship (VOS) measurements analyzed by *Lüger et al.* [2004] exhibited a pCO_2 variance of 23.8 μatm with a peak-to-peak amplitude of about 200 μatm. In the presence of such a high pCO_2 variability one cannot exclusively rely on simple interpolation between isolated local measurements. Alternative techniques need to be investigated to obtain reliable estimates of basin-wide pCO_2 on synoptic timescales. When targeting the monitoring of anthropogenic CO_2 fluxes, the accuracy of any pCO_2 estimate has to be quite high. For example, *Watson et al.* [1991] noted that a bias of 1 μatm in a global ΔpCO_2 (atmospheric pCO_2 minus sea surface pCO_2) estimate would result in an uncertainty in the

[1]Leibniz-Institut für Meereswissenschaften an der Universität Kiel (IfM-GEOMAR), Kiel, Germany.

[2]Now at International Pacific Research Center, School of Ocean and Earth Science and Technology, University of Hawai'i at Manoa, Honolulu, Hawaii, USA.

0148-0227/09/2007JC004646$09.00

Table 1. Vessels, Principal Investigators, and Reference Websites for VOS Line Data of the Year 2005 Used for Our Study

CarboOcean		
Ship	PIs/Chief Scientists	Reference for CarboOcean Data Portal[a]
Nuka Arctica	T. Johannessen A. Olsen	26na2005
Hespérides	A. F. Rios	29he2005
Poseidon	T. Steinhoff D. W. R. Wallace A. Körtzinger	06po2005
G. O. Sars	T. Johannessen A. Olsen	58gs2004
Trans Carrier	A. Omar	58tc2005
Santa Maria	U. Schuster A. Watson	64sa2005
Falstaff	T. Steinhoff D. W. R. Wallace A. Körtzinger	77ff2005
Quima	M. Gonzalez-Davila J. M. Santana-Casiano I. Rodriguez-Ucha	quima2005
US/American Partners		
Ship	PIs/Chief Scientists	Reference
R. H. Brown	R. Castle J. Shannahoff R. Wanninkhof	www.aoml.noaa.gov/ocd/gcc/index.php
Explorer	B. Huss R. Wanninkhof	www.aoml.noaa.gov/ocd/gcc/index.php
Skogafoss	K. Sullivan D. Pierrot R. Wanninkhof	www.aoml.noaa.gov/ocd/gcc/index.php

[a]http://dataportal.carboocean.org/front_content.php?idcat=142.

calculated ocean carbon uptake of ~0.2 Pg/a which is about 10% of the total uptake estimated by *Takahashi et al.* [2002].

[5] Ocean surface pCO_2 depends on sea level pressure, DIC, total alkalinity, sea surface temperature (SST) and salinity, of which currently only SST is observable by satellite-based remote sensing on a basin-wide scale. Thus a straightforward calculation of basin-wide pCO_2 is impeded by the limited data availability. In addition to SST, remote sensing of ocean color, from which one can estimate concentrations of surface chlorophyll (Chl), are typically delivered daily with, apart from cloudy and high-latitude winter scenes, essentially global coverage. These two remotely sensed data sets contain valuable information about the two main physical and biological drivers of the above variables determining pCO_2. Although approximative regressions may work well in some circumstances [*Watson et al.*, 1991; *Bates et al.*, 1995; *Lüger et al.*, 2004; *Lefèvre and Taylor*, 2002; *Lefèvre et al.*, 2005], a stringent algebraic relation between SST, Chl and pCO_2, does not exist. For SST, the simple temperature dependency of surface pCO_2 leading to a decrease in pCO_2 with decreasing SST is often superimposed by entrainment of DIC-rich water due to vertical mixing caused by a cooling of the ocean surface. The Chl-pCO_2 relation depends strongly on season. The spring bloom increase in Chl concentrations usually causes a significant decrease in pCO_2, whereas variations in summer Chl concentrations can be totally decoupled from pCO_2. Furthermore, the relationship between satellite-derived surface Chl and phytoplankton biomass is complicated and depends, among others, on the actual physiological state of the phytoplankton.

[6] In the present study we therefore explore the potential of nonalgebraically combining local VOS measurements of pCO_2 and related variables (SST, Chl) with global satellite data of SST and Chl (but not pCO_2) for generating high-resolution monthly maps of surface pCO_2 estimates for an entire ocean basin.

[7] VOS line-based sampling of pCO_2, SST and Chl is simulated in the framework of a high resolution biogeochemical circulation model of the North Atlantic. A neural network (Kohonen Feature Map, KFM) is trained with these synthetic "observations" to reproduce model-generated "measurements" of pCO_2 from SST and Chl along the modeled VOS lines. The KFM trained by the model-generated VOS line data is then applied on the basin scale to model-generated remote sensing data of SST and Chl. The accuracy of the resulting basin-wide pCO_2 maps is analyzed with regard to missing data due to clouds and low solar irradiation in winter, remote sensing errors, and spatio-temporal coverage of the VOS line data used to train the KFM.

[8] The paper is organized as follows: In the subsequent section we present the high-resolution biogeochemical circulation model. The procedure used to simulate VOS line sampling and remote sensing is described in section 3. Section 4 deals with the neural network and its configuration. The presentation and discussion of our results (section 5) is split into a simulation to test different scenarios without the interference of remote sensing data gaps, the handling of missing data in the remote sensing of SST and Chl, CO_2 fluxes calculated from pCO_2 estimates, and an evaluation of our method. Section 6 summarizes our results.

2. Model Configuration

[9] A pelagic nitrogen-based nutrient-phytoplankton-zooplankton-detritus ecosystem model is coupled to a high-resolution regional ocean general circulation model of the

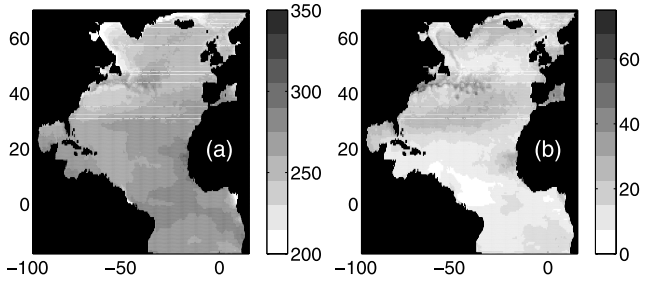

Figure 1. (a) Mean and (b) variance of modeled surface pCO_2 (in μatm) subsampled on 1/2° × 1/2° grid. Note the preindustrial atmospheric pCO_2 setup of the model.

North Atlantic. All ecosystem parameters as well as the equations determining the ecosystem dynamics are the same as those presented by *Oschlies et al.* [2000]. DIC and dissolved oxygen are coupled to nitrogen via the Redfield ratios, and alkalinity is diagnosed from a regional fit to salinity [*Eden and Oschlies*, 2006]. The underlying regional ocean circulation model is based on the modular ocean model MOM2 [*Pacanowski*, 1995]. The model domain spans the Atlantic Ocean from 18°S to 70°N at a horizontal resolution of 1/12° × 1/12° cos(latitude) and 45 vertical geopotential levels ranging from 10 m thickness near the surface to 250 m near the maximum depth of 5500 m. Surface boundary forcing consists of monthly mean wind stress, a Haney-type heat flux condition as given by *Barnier et al.* [1995], and a restoring condition for sea surface salinity. A sensitivity experiment was run with daily ECMWF forcing as described by *Eden and Jung* [2006]. Subgrid-scale parametrizations are biharmonic friction and diffusion (with biharmonic coefficients of 0.8×10^{10} m^4/s for diffusion and 2×10^{10} m^4/s for viscosity) and a level-1.5 closure scheme for vertical turbulent mixing following *Gaspar et al.* [1990].

[10] Initial conditions for nitrate are taken from the work of *Conkright et al.* [2002], and for DIC from the preindustrial estimate of the GLODAP data set [*Key et al.*, 2004]. The atmospheric pCO_2 remains on a preindustrial level, but varies seasonally and latitudinally according to a nonlinear fit to observational estimates by *Conway et al.* [2004]. The coupled biogeochemical-physical model is integrated over a 10 year spin-up period, and model data used here for simulating VOS line-based observations and remote sensing are taken from the model year 11. The annual mean and variance of simulated surface pCO_2 is shown in Figure 1.

3. Data

[11] The VOS line coverage of the North Atlantic in the year 2005 was, until then, the most comprehensive one in the VOS pCO_2 sampling history. Approximately 740,000 measurements had been gathered in the area 10°S to 70°N (∼ our model domain). The observational coverage maintained by the European project CARBOOCEAN and US/American partner projects, includes a monthly monitoring along the route UK-Caribbean, and also between the North Sea and the southern tip of Greenland (Figure 2; Table 1). Because of the lack of monthly coverage further south, we restricted the area considered in our study to the region north of 15°N. We also note that the VOS data of the year 2005 set does not contain any data points in the Labrador Sea. Consequently, no training data was available for the mapping of pCO_2 in this region of particular importance for the oceanic CO_2 uptake [*Sabine et al.*, 2004].

[12] Infrared and optical satellite data coverage is limited by clouds and, in the case of Chl, low solar irradiation at high latitudes in winter. Figure 2 indicates the number of days per month during which satellite data for Chl could be obtained by SeaWiFS for the year 2005. The data availability (for Chl) is typically less than 50% at every grid point for any month of the year, whereas almost no data is available for Chl north of 50°N in winter between November and February. In the following, we will sample the output of our high-resolution biogeochemical-circulation model with a sampling schedule that exactly follows the coverage of VOS lines and remote sensing data of the year 2005. Thus we do not use the actual observations but only the associated metainformation.

[13] To assess the reliability of our methodological study, we first check whether the temporal and spatial variability of the modeled pCO_2 is representative of real pCO_2 data. To this extent, we compare model-generated and observed pCO_2 variability along the VOS cruise tracks conducted by the carcarrier M/V Falstaff in the years 2002/2003 [*Lüger et al.*, 2004] encompassing a full annual cycle on 15 transits with more than 78,000 samples in the area between UK/Northern Spain and North America.

[14] The amplitude of the variations in pCO_2 is comparable for synthetic and actual measurements (Figure 3a). There is no phase relationship between the fluctuations since the stochastic nature of the variations overweighs the sea-

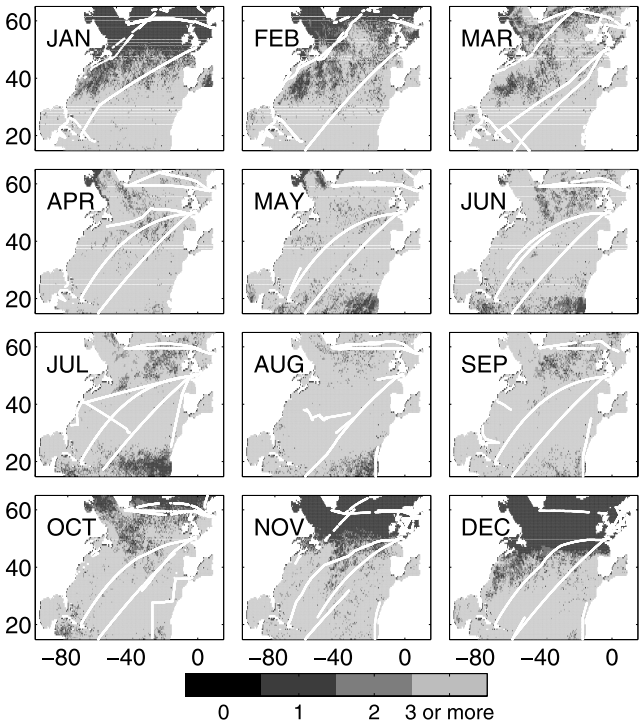

Figure 2. Availability of remote sensing data for chlorophyll (number of days per month) and monthly tracks of VOS lines for the year 2005 (white lines).

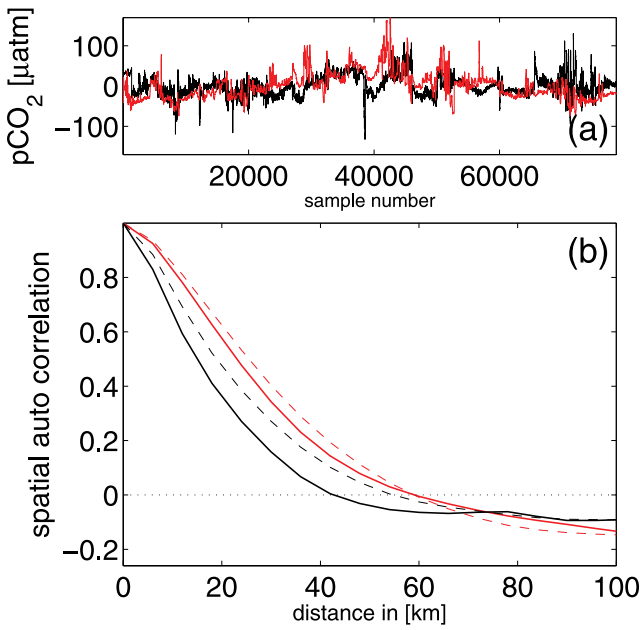

Figure 3. (a) Temporal pCO_2 variability for actual and model-generated measurements of carcarrier M/V Falstaff [*Lüger et al.*, 2004]: black, observed; red, model-generated. Because of the preindustrial atmospheric pCO_2 model setup, the mean was removed from each curve. (b) Corresponding mean along-track spatial autocorrelation scales (in km) for observed (black solid), model-generated (red solid) pCO_2 and observed (black dashed), model-generated (red dashed) SST.

sonal influences on this scale of sampling ($\leq$10 km). The sampling scale is typically smaller than the model grid spacing of $1/12^\circ \times 1/12^\circ$ cos(latitude). Thus for the analysis of along-track spatial scales, all observations falling into the same model grid box are averaged. Subsequently, model-generated and actual observations are linearly detrended and linearly interpolated onto the same grid of 7×7 km^2 corresponding to the model resolution at the mean latitude (40°N) of the M/V Falstaff cruises. On this grid, the pCO_2 variance amounts to 23.8 μatm for the actual observations and to 32.5 μatm for the model-generated "data," respectively.

[15] As expected, the mean spatial scales of the observed SST are larger than those of the observed pCO_2. This is relatively well reproduced by the model-generated data (Figure 3b). However, for both variables the mean spatial scales of the model-generated data in our model are larger than those of the real data. The spatial autocorrelation function crosses zero at 43 km for the real and at 59 km for the synthetic data. A possible reason for the too large scales in the model might be the absence of a diurnal cycle and the use of climatological forcing in the model, leading to less smallscale variability for the model-generated data. Overall, the calculated scales are significantly shorter than those presented by *Murphy et al.* [2001] who analyzed pCO_2 autocorrelation scales in the Gulf of Alaska and *Li et al.* [2005] who analyzed mean global autocorrelation scales of pCO_2 for the period 1970–2003. Compared to *Murphy et al.* [2001] the shorter scales found in our analysis can be explained by the higher eddy activity in the North Atlantic [*Chelton et al.*, 2007]. The different timescales considered may explain the differences with respect to the study by *Li et al.* [2005].

4. Methods

[16] Estimating basin-wide pCO_2 from remotely sensed SST and Chl requires a formulation which converts the two observed quantities (SST, Chl) into pCO_2. Finding such a relationship between pCO_2 and SST and/or Chl has been subject of previous studies [*Watson et al.*, 1991; *Bates et al.*, 1995; *Lüger et al.*, 2004; *Lefèvre and Taylor*, 2002; *Lefèvre et al.*, 2005]. Nevertheless, an exact mathematical relationship $\overline{pCO_2}$ = f(SST, Chl) or $\overline{pCO_2}$ = f(SST, Chl, Position, Time) does not exist as pCO_2 depends on other factors than local SST and Chl. Surface waters with identical SST and Chl can well have different pCO_2 levels. For the context of simple linear functional relationships, this can be illustrated by applying a multiple linear regression to the model-generated data:

$$pCO_2 = \mathrm{A} \cdot SST + \mathrm{B} \cdot Chl + \mathrm{C} \qquad (1)$$

with the coefficients A, B and C being functions of space and time. For computational reasons, the model data were subsampled on a grid of $1/2^\circ \times 1/2^\circ$ resolution. The regression coefficients A(Lat,Lon,Month) (Figure 4) and B(Lat,Lon,Month) (not shown) exhibit considerable variability both in time and in space. Spatial gradients in the SST coefficient A(Lat,Lon,Month) can reach values up to 60 μatm/°C/100 km whereas temporal fluctuations easily exceed $\pm$20 μatm/°C in a month. This makes it difficult to envisage some division of the North Atlantic into seasonal or regional biogeophysical regimes with constant regression coefficients.

[17] In contrast to standard regression techniques, Kohonen Feature Maps (KFMs) [*Kohonen*, 1982] work as an associative memory that can be used to estimate pCO_2 from SST and Chl (and position in time and space) without fitting a predefined mathematical function. The concept of KFMs is motivated by neurobiological findings about the topological organization of sensory experiences in certain areas of the brain. The KFM consists of a topological arrangement of neurons that associate an input vector (here SST, Chl, position, time) with an output (here pCO_2). Similar to the brain, a KFM has to learn how to associate input and output. This is achieved by confronting the KFM with "stimulus" pairs of input and output variables in a training process. A detailed description of the formation of topological maps during the training process can be found in the works of *Kohonen* [1982] and *Lefèvre et al.* [2005]. Figure 5 illustrates a simple scheme of the functioning. In the training process the mean topological features of the observed combinations [SST, Chl, pCO_2] are memorized in a map of (normalized) vectors and corresponding pCO_2 values. In the application process, an input vector (normalized SST and Chl in the example of Figure 5) is associated with the pCO_2 value belonging to the best fitting vector of the parameter space representation.

[18] In our case, model-generated VOS line samples of SST and Chl and corresponding Latitude, Longitude, Day (in the year) are used to form a five-dimensional parameter space representation in the training process. In the subsequent application phase the KFM can associate

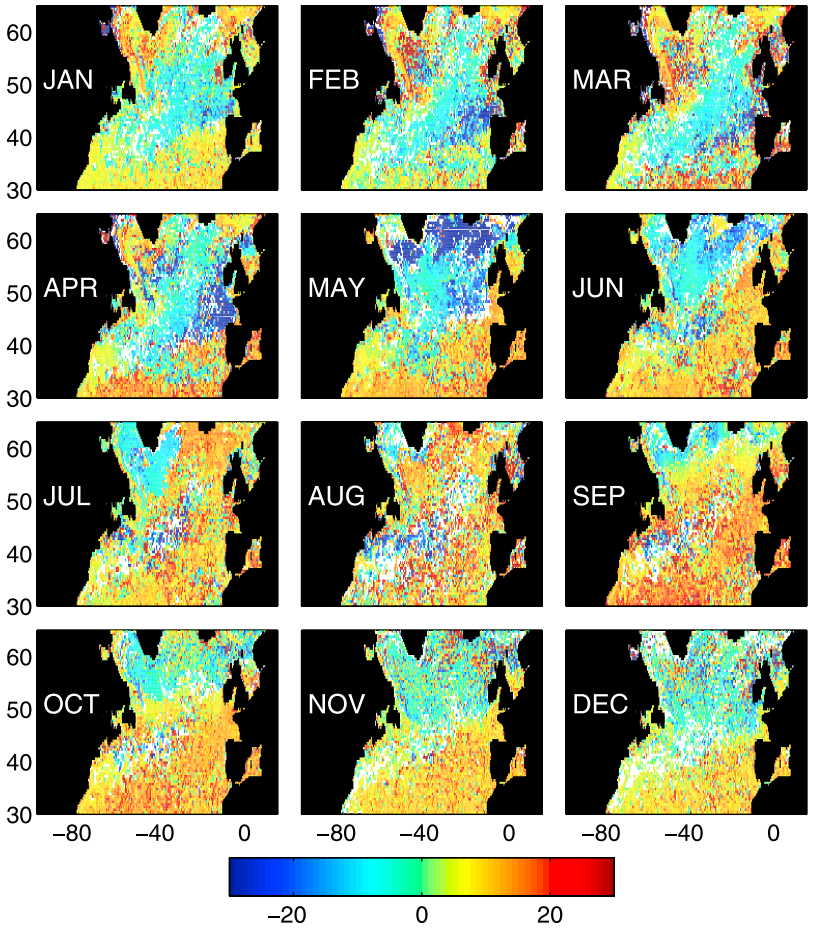

Figure 4. Regression coefficients of model-generated pCO_2 versus model-generated SST (in μatm/°C) for a multiple linear regression applied monthly to the model data on a 1/2° × 1/2° grid according to equation (1). White areas indicate regions where the multiple linear regression accounts for less than 50% of the model-generated pCO_2 variance.

simulated remote sensing data of SST and Chl (and the respective position and time) with a pCO_2 value. Input data was normalized as follows:

$$Day' = \cos\frac{Day \cdot 2\pi}{365} \tag{2}$$

$$Lat' = \frac{latitude - 15°N}{65°N - 15°N} \tag{3}$$

(only data between 15°N and 65°N were considered)

$$Lon' = \frac{longitude - 88°W}{11°E - 88°W} \tag{4}$$

$$SST' = \frac{SST - \overline{SST}}{STD(SST)} \tag{5}$$

$$Chl' = \frac{log(Chl + 0.01) - \overline{log(Chl + 0.01)}}{STD(log(Chl + 0.01))} \tag{6}$$

Overlined variables refer to the spatial-temporal average.

[19] The input for "Day" was normalized sinusoidally, following *Lefèvre et al.* [2005] and emphasizing the seasonal cycle and allowing January to be close to both February and December. A lognormal distribution was assumed for model-generated Chl following *Campbell* [1995]. A value of

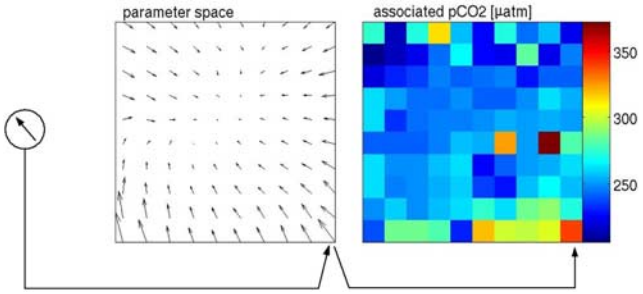

Figure 5. Schematic mode of operation of a trained KFM. An (left) input vector is associated with (right) the pCO_2 value of (center) the best matching vector of the parameter space representation. x and y axes denote (dimensionless) width of KFM. Note: For clarity, the dimension of the KFM was reduced to a 10 × 10 array of neurons, and the input (and parameter) space was chosen to be two-dimensional only (e.g., SST and Chl).

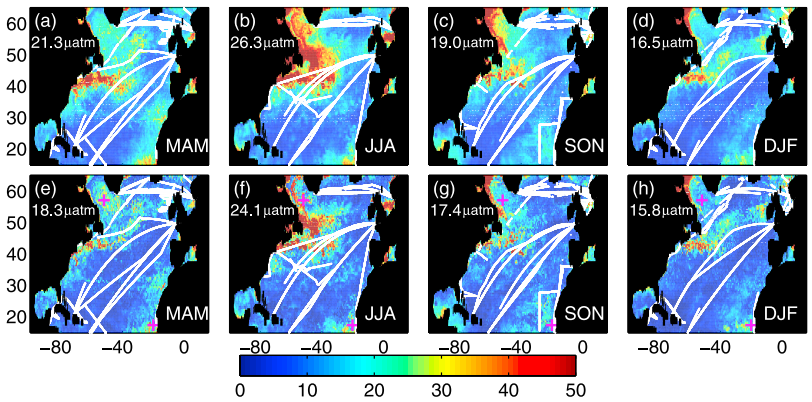

Figure 6. Seasonal mean RMS error (in μatm) for mapping based on model-generated VOS lines of the year 2005 (white lines) and (a–d) daily or (e–h) monthly mean model-generated remote sensing data of SST and Chl. Magenta crosses in the Labrador Sea and off West Africa in Figures 6e–6h denote positions of two simulated stationary monitoring buoys (see text for details).

0.01 $\frac{mgChl}{m^3}$ has been added to avoid a large impact of data uncertainties at very low Chl concentrations.

[20] Since a KFM works as an associative allocation between parameter vectors and target values, the number of combinations [pCO_2,SST,Chl,Day,Lat,Lon] that are set during the training process and later used as "look-up table" to estimate pCO_2 from the input variables [SST,Chl,Day, Lat,Lon] is restricted by the size of the map. By choosing a map that is too small (i.e., a too small number of neurons), it would not be possible to adequately represent all features of the training data. The map would already be occupied by the dominating features, leaving no room for more infrequently sampled regions or events, such as the West African upwelling. In order to find an optimal size for the topological map, we trained 16 KFMs (20×20, 40×40, ..., 320×320 neurons) with the synthetic observations (SST, Chl and corresponding Day, Lat, Lon) of the model-generated VOS lines and reconstructed surface pCO_2 from model-generated remote sensing data of SST and Chl (and corresponding Day, Lat, Lon). Missing data due to a lack in optical satellite coverage were not considered in this case. The basin-wide RMS error of the estimated pCO_2 as a function of the map size shows a substantial decrease of the mapping error on increasing the number of neurons from 20×20 to 220×220, and a slightly increasing RMS error thereafter.

[21] Nowadays, remote sensing of SST and Chl is normally available at a spatial resolution of approximately 9 km (SeaWiFS). For computational reasons, we subsampled the model-generated remote sensing data on a somewhat coarser $1/2° \times 1/2°$ grid. The impact of remote sensing errors on the pCO_2 estimates was investigated by adding Gaussian noise with $\sigma = 0.5$ K to the model-generated SST data, and Gaussian nose with a variance of $\sigma = 30\%$ to the actual model-generated Chl data.

5. Results and Discussion

[22] With respect to possible efforts to monitor CO_2 sources and sinks, a monthly resolution of basin-wide pCO_2 maps seems to be a reasonable goal. In the following, our assessment will therefore focus on the accuracy of monthly maps of pCO_2 estimated from model-generated remote sensing data of SST and Chl via a KFM trained by model-generated VOS data. Because we restrict ourselves to synthetic observations, we can reliably assess the quality of

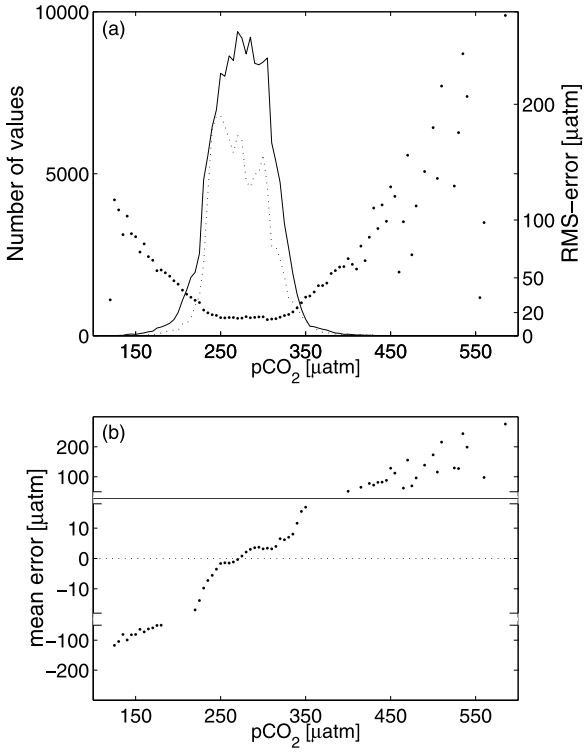

Figure 7. (a) Number of values in basin-wide modeled pCO_2 (solid line) and model-generated VOS line data of the year 2005 (dotted) and RMS error (in μatm; dots) versus modeled pCO_2 (in μatm; 5-μatm intervals). (b) Mean error of estimated pCO_2 (in μatm; dots) versus modeled pCO_2 (in μatm; 5-μatm intervals). Mapping based on simulated VOS lines of the year 2005 and monthly mean model-generated remote sensing data of SST and Chl. Note the split y axis in Figure 7b and the preindustrial atmospheric pCO_2 setup of the model.

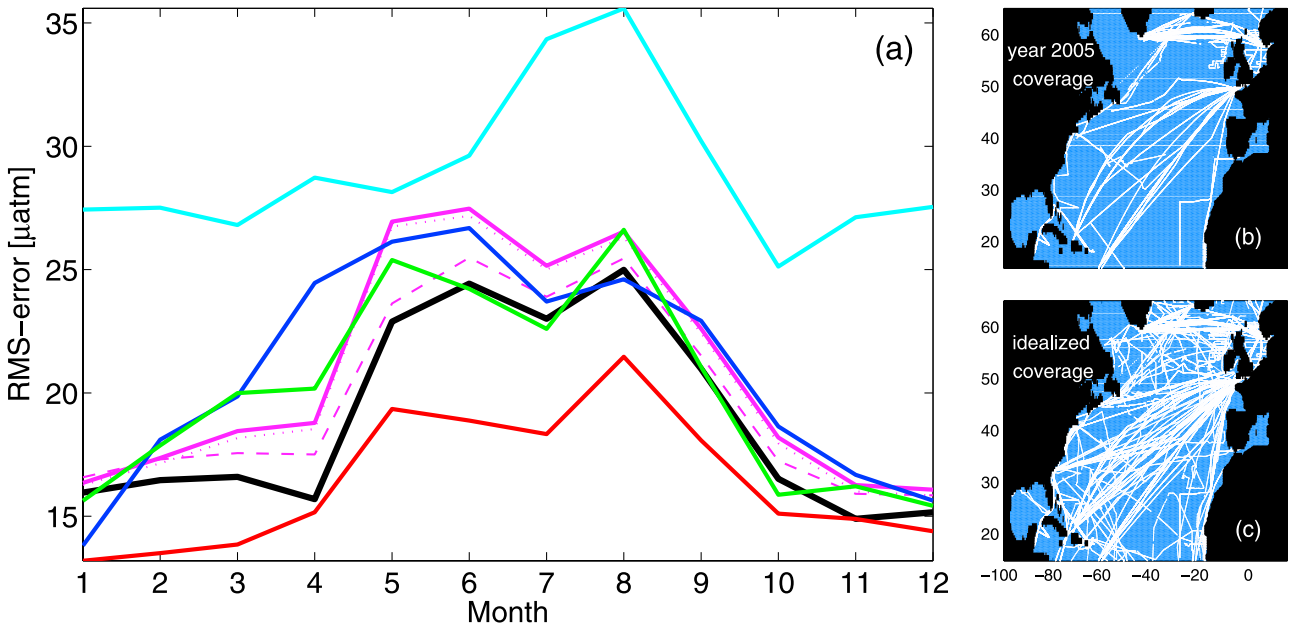

Figure 8. (a) Annual cycle of RMS error (in μatm) for basin-wide (15–65°N) mapping of pCO_2. Magenta, mapping based on simulated VOS lines of the year 2005 and daily remote sensing of SST and Chl when perfect satellite coverage is assumed (solid), as well as neglecting remote sensing errors in SST (dotted) and Chl (dashed); black, mapping based on simulated VOS lines of the year 2005 and monthly mean remote sensing data of SST and Chl disregarding missing data (reference simulation); green, similar to black, but remote sensing of Chl for training instead of onboard sampling; cyan, similar to black, but using only SST and Chl and not position and day; blue, similar to black, but using SST and position only; red, training and mapping based on an simulated idealized VOS line coverage. (b and c) Annual VOS lines coverage of the year 2005 and idealized coverage.

our pCO_2 estimates with respect to the known "true" pCO_2 simulated by the biogeochemical circulation model. This would not be possible for pCO_2 estimates from real satellite data as, in that case, the true pCO_2 is not known apart from a few data points (e.g., VOS lines) that would generally be used to train the KFM.

[23] Our methodological study and the analysis of our results focuses on the following questions:

[24] 1. What is the accuracy of basin-wide maps of surface pCO_2 for present-day VOS line coverage and how sensitive is this accuracy to changes in VOS coverage?

[25] 2. What is the impact of errors in the remotely sensed SST and Chl data?

[26] 3. What is the impact of incomplete remote sensing coverage and how can data gaps be interpolated?

[27] 4. What is the accuracy of CO_2 fluxes calculated from estimated pCO_2 maps?

[28] A first issue addresses the KFM mapping frequency needed to generate robust monthly mean pCO_2 estimates. Since remotely sensed SST and Chl are available on a daily basis, at least two alternative ways are conceivable of how to apply the data to the KFM. As a first option, daily values of SST and Chl can be converted by the KFM into daily values of pCO_2, which are subsequently averaged into monthly means. As a second option, monthly means of remotely sensed SST and Chl can be applied to the KFM to directly estimate monthly mean pCO_2 maps.

[29] Figure 6 shows a comparison of the seasonally averaged RMS error in the estimated pCO_2 maps for the two methods. For the top panels (a–d), pCO_2 was calculated from model-generated daily SST and Chl, and for the bottom panels (e–h), pCO_2 was estimated from model-generated monthly mean SST and Chl satellite data. For all seasons the mapping error turned out to be larger when model-generated daily SST and Chl data were used. Initially, this result seems counterintuitive: The KFM was trained to reproduce simulated in situ pCO_2 from model-generated instantaneous in situ SST and Chl data, and the mapping process is a nonlinear one: $pCO_2(\overline{SST}, \overline{Chl}) \neq \overline{pCO_2}$. Two features help to understand this counterintuitive behavior. The pCO_2 training data of the model-generated VOS lines as well as the model-generated "true" pCO_2 in the considered domain are distributed nearly normally (Figure 7a, dashed and solid lines), with most values concentrated in the interval of 230–330 μatm (note the preindustrial setup of the model). In this central pCO_2 range, the KFM resolves features most precisely, whereas it tends to overestimate (underestimate) lower (higher) pCO_2 values (Figure 7b). Largest mapping errors occur for pCO_2 <200 μatm and for >400 μatm (Figures 7a and 7b, dots). Particularly in areas of large gradients, e.g., in the North Atlantic Current (NAC) region close to the Grand Banks, where high pCO_2 values of the NAC encounter fairly low values of the Labrador Current, the KFM is not able to resolve such a high spatial variability. If the input data for the mapping consists of monthly mean values, these gradients are weaker.

[30] The remote sensing errors of SST and Chl provide the second reason, leading to a deviation when the KFM is

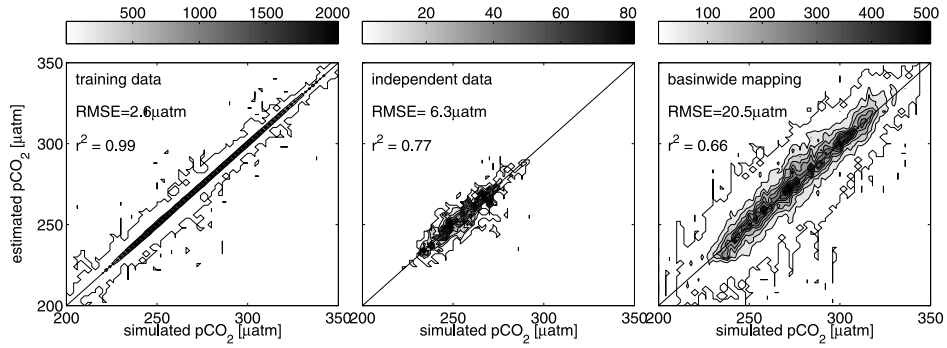

Figure 9. Comparison of model-generated "true" and estimated pCO_2 in numbers of data for (left) reproduction of training data, (center) reproduction of an model-generated independent data set, and (right) basin-wide (15–65°N) mapping corresponding to Figures 6e–6h and Figure 7. Note that given basin mean RMS error in the right panel is non-area-weighted. The associated area-weighted basin mean RMS error amounts to 19 μatm.

applied. As these errors are assumed to be of stochastic nature they tend to average out over the course of one month, resulting in more reliable monthly mean values. Significantly larger errors of the daily mapping in the Labrador Sea and Grand Banks region in summer (Figures 6b and 6f) can be attributed to the remote sensing errors for model-generated Chl. A more detailed analysis reveals a marginal and consistently smaller mapping error over the year for a perfect remote sensing of SST (Figure 8a, magenta dotted). With regard to a perfect remote sensing of Chl (Figure 8a, magenta dashed) a substantial improvement is primarily found for the months May to August.

[31] In a number of sensitivity experiments we also investigated the importance of the individual data sets for accurately estimating surface pCO_2. Even though a straightforward relation between Chl concentrations and pCO_2 does not exist, disregarding model-generated Chl observations (both in the training and in the application of the KFM) leads to considerably larger mapping errors, in particular during the spring bloom between February and June (Figure 8a, blue line).

[32] The same holds for neglecting position in time and space. Use of these coordinates in the mapping procedure appears unfounded at first sight and impedimentary for a theoretical insight into the dependence of pCO_2 on physical and biological parameters. However, an attempt to use only model-generated SST and Chl as input variables was not successful (Figure 8a, cyan line). Adding simulated mixed layer depth to the training and KFM input data (neglecting that there is no currently known method available to accurately determine mixed layer depth remotely) could not improve this result substantially.

[33] Figure 8a (green line) additionally shows the importance of measuring Chl onboard along the VOS lines instead of gathering training data through remote sensing. When remotely sensed Chl data with their relatively large errors are used in the training process, the topology of the KFM is deteriorated by the remote sensing errors which leads to larger mapping errors compared to more accurate in situ training data.

[34] Even for the case with model-generated in situ Chl training data and monthly mean remotely sensed SST and Chl, estimated pCO_2 still shows large errors in various regions (Figures 6e–6h and Figure 8a, black line). Beside the fact that unreproducible large gradients can still occur in monthly mean values of pCO_2, these mapping errors arise from the VOS line coverage of the year 2005 which, notwithstanding all endeavors, still has to be regarded as sparse. Large mapping errors in the Labrador Sea and around the Grand Banks (particularly in summer) do not necessarily indicate a deficiency of the method but can be seen as a consequence of the lack of training data in this area.

[35] A more detailed analysis of the errors in the estimated pCO_2 maps confirms that these are largest in areas far away from any training data set. As shown by Figure 9, the KFM can accurately reproduce the training data set with an RMS error of 2.6 μatm, while the errors are already more than twice as large along individual VOS lines excluded from the training data set (Figure 9, center). For the entire basin, however, the RMS error of the estimated pCO_2 field amounts to 20.5 μatm (area-weighted: 19 μatm). In contrast to our model study, in which the "true" pCO_2 of the model is known, the latter error would be difficult to estimate for real applications of the methods using real data. The conventional error assessment along individual VOS lines not contained in the training data is not necessarily indicative of the basin-wide error (Figure 9, center and right).

5.1. Impact of Spatial Resolution

[36] In order to add training data in regions with particularly large errors in the estimated pCO_2, two stationary monitoring buoys were additionally simulated in the model at the positions of 17°N/20°W close to the West African upwelling and at 57°N/55°W in the Labrador Sea (Figures 6e–6h, magenta crosses). A weekly sampling of local SST and pCO_2 together with remote sensing of Chl was assumed and added to the VOS line data for the training of the KFM. A clear regional improvement of the pCO_2 estimates was observed for the Labrador Sea buoy leading to a local 20% decrease of the RMS error, though having no significant effect in the basin-wide RMS error. For the simulated West African buoy the regional decrease in the error of the estimated pCO_2 was smaller. It was also limited to a

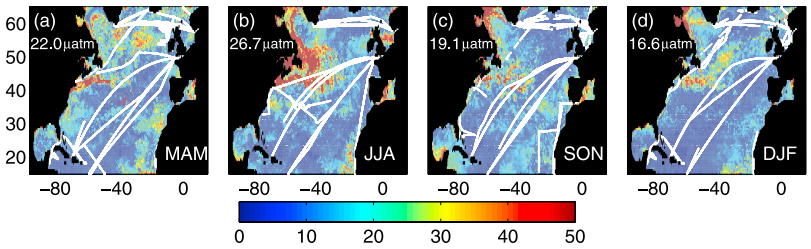

Figure 10. Seasonal mean RMS error (in μatm) for mapping based on simulated VOS lines and remote sensing of SST and Chl of the year 2005. Missing data caused by cloud cover or low solar irradiation were replaced by model-generated climatological values of SST and Chl. Seasonal VOS lines of the year 2005 (white lines).

significantly smaller area and even accompanied by an error increase in the surrounding region. This slight increase was caused by the fact that the observed pCO_2 values and biological and physical properties vary on small scales. Still, in the absence of sufficient surrounding observations, simulated local buoy data are taken as the best guess for the whole area by the KFM. The effect of both simulated buoys on the KFM estimate of pCO_2 could be greatly enhanced by an associated spatial variability study.

[37] In order to assess the potential of enhanced VOS sampling, the KFM was trained with a simulated idealized VOS line coverage. It was assumed that in addition to VOS lines of the year 2005, all freely accessible lines (http://cdiac.ornl.gov/oceans/pCO2inv.html) would have been occupied in the same year. The area-weighted, basin-wide annual mean RMS error can be reduced to 16.4 μatm in this case, compared to 19 μatm for the actual lines of the year 2005 (Figure 8a, red line).

5.2. Impact of Optical Satellite Coverage

[38] As discussed previously in section 3, remote sensing of ocean color and SST is limited by cloud cover and, in the case of ocean color, by low solar irradiation in winter. Hence the treatment of missing satellite data needs to be investigated. Basically, missing data can be replaced in two ways: Climatological values of SST and Chl might be used as input data for the KFM, or climatological pCO_2 could complete a mapping which is applied only to optically covered pixels. Both alternatives have been analyzed. Climatological pCO_2, SST and Chl were simulated by a model run with slightly different forcing (daily forcing for the considered year instead of monthly mean forcing) to account for possible biases in our climatologies. Simulated SST and Chl climatologies were assumed to be available on a $1/2^\circ \times 1/2^\circ$ grid. For the simulated pCO_2 climatology we have chosen the Takahashi [*Takahashi et al.*, 1997] resolution of $4^\circ \times 5^\circ$. Figure 10 illustrates the seasonally averaged RMS error for a mapping that replaces missing data in the remote sensing with climatological SST and Chl. Mapping errors are similar to those obtained earlier for the idealized case of no missing data (Figures 6e–6h). Comparing the annual cycle of the errors (Figure 11) with the missing data ratio (Figure 2) does not reveal a correlation of the error size with optical coverage, which is lowest in winter. Instead, errors of the estimated pCO_2 fields are largest in summer, similar to the earlier simulation that assumed no missing data.

[39] Overall, it becomes apparent that the mapping errors are dominated by the method's inability to reproduce areas of large pCO_2 gradients whereas the replacement of missing data is of secondary importance. In our simulation, substituting gaps in optical satellite coverage by model-generated climatological pCO_2 achieves better results than using model-generated climatological SST and Chl input variables to the KFM (Figure 11). However, it should be kept in mind that real-world climatological pCO_2 under increasing atmospheric CO_2 levels is still afflicted with considerable uncertainties, which was neglected in our preindustrial simulation.

5.3. CO_2 Fluxes

[40] One major reason for estimating basinscale pCO_2 maps is the assessment of marine CO_2 uptake. Air-sea gas exchange is, besides the variation from the equilibrium pCO_2 value, a function of the gas transfer velocity (piston velocity). This piston velocity is here assumed to depend quadratically on wind speed, following the work of *Wanninkhof* [1992]. As a result, temporal and spatial patterns of error in CO_2 fluxes calculated from estimated pCO_2 do not necessarily resemble RMS error patterns shown in Figures 6 and 10. In fact, errors in estimated wintertime pCO_2 tend to cause larger errors in CO_2 fluxes whereas errors in the summer, which dominate in our simulations, will have a minor effect.

[41] In our simulation the annual cycle of the model-generated "true" CO_2 fluxes is very well reproduced in the considered region 15°N to 65°N when CO_2 fluxes are calculated from the mapped pCO_2 replacing missing data

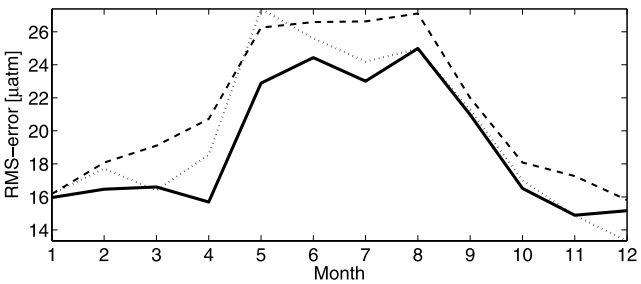

Figure 11. Annual cycle of RMS error (in μatm) for basinwide (15–65°N) mapping of pCO_2 for an assumed perfect satellite coverage (solid) and for a replacement of missing data by model-generated climatological pCO_2 (dotted) and model-generated climatological SST and Chl (dashed).

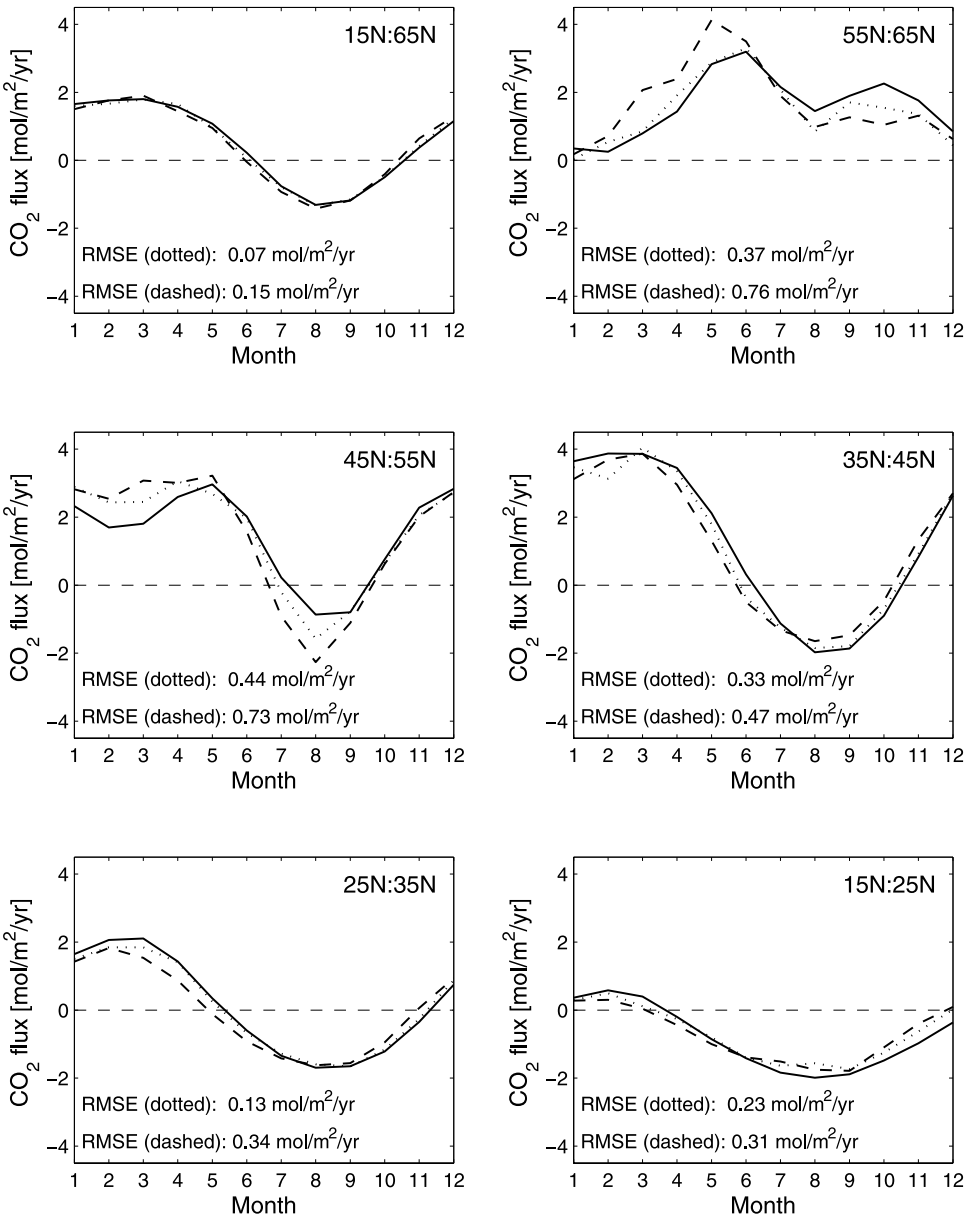

Figure 12. Annual cycle of model-generated "true" (solid) and estimated CO_2 fluxes, replacing missing data in the simulated remote sensing with model-generated climatological SST and Chl (dashed) and for assumed perfect satellite coverage (dotted) for given latitudes (in mol/m^2/a). CO_2 fluxes were calculated using the piston velocity formulation of *Wanninkhof* [1992]. Positive values denote fluxes into the ocean.

in the remote sensing with simulated climatological SST and Chl (Figure 12, top left). The RMS error of monthly and regionally averaged CO_2 fluxes amounts to 0.15 mol/m^2/a. The amplitude of the seasonal cycle of the estimated flux amounts to 3.3 mol/m^2/a (3.1 mol/m^2/a when we assume perfect satellite coverage) and overestimates the model-generated "true" amplitude by 6.8%.

[42] Regionally, significant deviations from the model-generated "true" CO_2 flux (Figure 12) and CO_2 uptake (Table 2) can occur. Largest errors in CO_2 flux are found in the North Atlantic Current region from December to April (where the main uptake takes place in our model) and derive from errors in the estimated pCO_2 in this region of large pCO_2 gradients. Errors in CO_2 fluxes are also elevated by the replacement of missing data due to cloud cover and low solar irradiation in late fall and winter. In the regions 25°N to 35°N and north of 55°N, as well as in the basin-wide mean, more than half of the RMS error of monthly and regionally averaged CO_2 fluxes derives from the substitution of missing data. In particular north of 55°N, CO_2 uptake is overestimated for the months March to May which is caused by an overestimate of the pCO_2 drawdown. This overestimate is not found in the simulation without missing data and is caused by too high synthetic climatological Chl values taken as a replacement for the missing data. Whether disregarding or replacing missing data in the

Table 2. Area-Weighted RMS Error, Model-Generated "True" CO_2 Uptake (in TgC/a) and Deviation From Simulated "True" CO_2 Uptake (Model-Generated "True" CO_2 Uptake − Estimated CO_2 Uptake; in TgC/a) for pCO_2 Mapping Replacing Missing Data in the Simulated Remote Sensing With Model-Generated Climatological SST and Chl[a]

Region	Area-Weighted Mean RMS Error (μatm)	Model-Generated "True" CO_2 Uptake (TgC/a)	Model-Generated "True" CO_2 Uptake − Estimated CO_2 Uptake (TgC/a)
15°N:65°N	21.1	190.6	+11.5
55°N:65°N	24.4	78.5	−3.6
45°N:55°N	25.8	81.7	+2.5
35°N:45°N	25.7	102.1	+8.9
25°N:35°N	15.2	13.0	+11.4
15°N:25°N	18.9	−84.6	−7.7

[a]CO_2 fluxes were calculated using the piston velocity formulation of *Wanninkhof* [1992].

remote sensing, errors in estimated CO_2 fluxes are not in phase with pCO_2 mapping errors but have a maximum in winter when errors in the estimated pCO_2 maps are comparatively low.

5.4. Method Evaluation

[43] When evaluating the presented method it is important to distinguish between different objectives of a basin-wide pCO_2 mapping and thus between local mapping errors and basin mean errors. As local mapping errors are large in various regions it is not clear whether the presented method can reliably detect interannual fluctuations and trends in the considered areas and hence provide a benefit compared to a simple use of a pCO_2 climatology. For the basin mean view, however, we do believe that there is additional benefit. *Lüger et al.* [2004] found climatological pCO_2 values [*Takahashi et al.*, 2002] to be on average lower than observed values by 13 μatm in the eastern basin (35°W to 0°W) of the North Atlantic and to be, on average, higher by 2 μatm for the western part (80°W to 35°W). For the eastern part the differences were dominated by deviations of up to 22 μatm between January and May. In comparison, for our method we find basin mean differences (model-generated "true" pCO_2 − estimated pCO_2) of −2.1 μatm (1.8 μatm) for the western (eastern) part with maximum monthly deviations of 9.5 μatm.

[44] The model-generated basin mean pCO_2 is overestimated by 0.51 μatm by the KFM mapping technique with missing remote sensing data replaced by climatological SST and Chl values. Taking into account ΔpCO_2 values (atmospheric pCO_2 − sea surface pCO_2) of 26 μatm in the mid-1990s and 5 μatm in the early 2000s as reported by *Schuster and Watson* [2007] for the region 20°N to 65°N, this estimated basin mean error is still about one order of magnitude smaller than observed decadal changes. In our simulation the slight overestimate of basin mean pCO_2 leads to an underestimate of basin-wide CO_2 uptake by 6.0% (Table 2) which is a promising value. However, it must be kept in mind that the accuracy of the presented method strongly depends on the relationships between SST, Chl and pCO_2. In particular for Chl which, in the model is simply a constant fraction of phytoplankton biomass, this relationship is likely to be more complex in the real ocean. Other aspects that have been neglected in the current model are effects of calcium carbonate forming organisms on alkalinity and hence pCO_2, as well as variations in the carbon-to-nutrient ratios of organic matter.

6. Conclusions

[45] By simulating present-day observational sampling schemes in the context of an eddy-resolving biogeochemical circulation model, we have demonstrated that VOS line measurements and satellite data can be combined by a self-organizing neural network in order to generate monthly basin-wide maps of pCO_2. Our results show that, besides the still insufficient VOS line coverage and the frequent occurrence of missing data in the remote sensing of SST and Chl, the high spatial variability of pCO_2 in the NAC region is the most crucial limiting factor for the accuracy of the mapping procedure suggested here for the North Atlantic. The basin-wide RMS error for a hypothetical perfect satellite coverage (or a hypothetical perfect scheme to interpolate missing data due to clouds and low solar irradiation in winter) amounts to 19.0 μatm, but reaches locally 50 μatm and more in the region of large pCO_2 gradients, even though training data and an independent data set can be reproduced with a much lower RMS error of 2.6 μatm 6.3 μatm respectively.

[46] Compared to model-generated daily data of remotely sensed SST and Chl, synthetic monthly mean data of SST and Chl provide a more reliable and successful basis for producing basin-wide pCO_2 charts since remote sensing errors and large pCO_2 gradients are reduced. Simulating the VOS lines and actual optical satellite coverage of the year 2005, a basin-wide mean RMS error of 21.1 μatm is found when missing data in the remote sensing are replaced by model-generated climatological values of SST and Chl. The annual cycle of the model-generated "true" CO_2 fluxes can be well reproduced from the estimated pCO_2. The amplitude of the annual cycle is slightly overestimated by 6.8% while the basin-wide CO_2 uptake is underestimated by 6.0%.

[47] The extension of monitoring pCO_2 is highly recommended as our results indicate a significant improvement in the basinscale pCO_2 maps for an increased VOS line coverage. For this purpose, more observations would be particularly useful in the Labrador Sea and the NAC area. The additional use of float-based pCO_2 sampling might provide a substantial benefit.

[48] **Acknowledgments.** Our thanks go first to the numerous scientists and personnel responsible for the collection of VOS line and SeaWiFS data that form the basis of our model simulation. We are grateful to C. Eden for running the biogeochemical ocean model. We also thank the anonymous reviewers for their helpful comments. This work was funded by the European Union via CarboOcean 511176 (GOCE). This is International Pacific Research Center contribution 581 and School of Ocean and Earth Science and Technology contribution 7619.

References

Barnier, B., L. Siefridt, and P. Marchesiello (1995), Surface thermal boundary condition for a global ocean circulation model from a three-year climatology of ECMWF analyses, *J. Mar. Syst.*, *6*, 363–380.

Bates, N. R., A. F. Michaels, and A. H. Knap (1995), Seasonal and interannual variability of oceanic carbon dioxide species at the U.S. JGOFS Bermuda Atlantic Time-series Study (BATS) site, *Deep Sea Res.*, *Part II*, *43*, 347–383.

Campbell, J. W. (1995), The lognormal distribution as a model for bio-optical variability in the sea, *J. Geophys. Res.*, *100*(C7), 13,237–13,254.

Chelton, D. B., M. G. Schlax, R. M. Samelson, and R. A. de Szoeke (2007), Global observations of large oceanic eddies, *Geophys. Res. Lett.*, *34*, L15606, doi:10.1029/2007GL030812.

Conkright, M. E., H. E. Garcia, T. D. O'Brien, R. A. Locarnini, T. P. Boyer, C. Stephens, and J. I. Antonov (2002), *World Ocean Atlas 2001, vol. 4: Nutrients*, edited by S. Levitus, *NOAA Atlas NESDIS 54*, 392 pp., U.S. Govt. Print. Off., Washington, D. C.

Conway, T. J., P. P. Tans, L. S. Waterman, K. W. Thoning, D. R. Kitzis, K. A. Masarie, and N. Zhang (1994), Evidence for interannual variability of the carbon cycle from the National Oceanic and Atmospheric Administration/Climate Monitoring and Diagnostics Laboratory Global Air Sampling Network, *J. Geophys. Res.*, *99*(D11), 22,831–22,855.

Eden, C., and T. Jung (2006), Wind driven eddies and plankton blooms in the North Atlantic Ocean, *Tech. Memo. 490*, ECMWF, Reading, U. K.

Eden, C., and A. Oschlies (2006), Adiabatic reduction of circulation-related CO_2 air-sea flux biases in a North Atlantic carbon-cycle model, *Global Biogeochem. Cycles*, *20*, GB2008, doi:10.1029/2005GB002521.

Gaspar, P., Y. Gregoris, and J.-M. Lefèvre (1990), A simple eddy kinetic energy model for simulation of the oceanic vertical mixing: Tests at station Papa and long-term upper ocean study site, *J. Geophys. Res.*, *95*(C9), 16,179–16,193.

Key, R. M., A. Kozyr, C. L. Sabine, K. Lee, R. Wanninkhof, J. L. Bullister, R. A. Feely, F. J. Millero, C. Mordy, and T.-H. Peng (2004), A global ocean carbon climatology: Results from Global Data Analysis Project (GLODAP), *Global Biogeochem. Cycles*, *18*, GB4031, doi:10.1029/2004GB002247.

Kohonen, T. (1982), Self-organized formation of topologically correct feature maps, *Biol. Cybern.*, *43*, 59–69.

Lefèvre, N., and A. Taylor (2002), Estimating pCO_2 from sea surface temperatures in the Atlantic gyres, *Deep Sea Res. I*, *49*, 539–554.

Lefèvre, N., A. J. Watson, and A. R. Watson (2005), A comparison of multiple regression and neural network techniques for mapping in situ pCO_2 data, *Tellus*, *57*, 375–384.

Li, Z., D. Adamec, T. Takahashi, and S. C. Sutherland (2005), Global autocorrelation scales of the partial pressure of oceanic CO_2, *J. Geophys. Res.*, *110*, C08002, doi:10.1029/2004JC002723.

Lüger, H., D. W. R. Wallace, A. Körtzinger, and Y. Nojiri (2004), The pCO_2 variability in the midlatitude North Atlantic Ocean during a full annual cycle, *Global Biogeochem. Cycles*, *18*, GB3023, doi:10.1029/2003GB002200.

Murphy, P. P., Y. Nojiri, D. E. Harrison, and N. K. Larkin (2001), Scales of spatial variability for surface ocean pCO_2 in the Gulf of Alaska and Bering Sea: Toward a sampling strategy, *Geophys. Res. Lett.*, *28*(6), 1047–1050.

Oschlies, A., W. Koeve, and V. Garçon (2000), An eddy-permitting coupled physical-biological model of the North Atlantic: 2. Ecosystem dynamics and comparison with satellite and JGOFS local studies data, *Global Biogeochem. Cycles*, *14*(1), 499–523.

Pacanowski, R. (1995), MOM 2 documentation user's guide and reference manual, *Tech. Rep. 3*, 232 pp., GFDL Ocean Group, GFDL, Princeton, N. J.

Sabine, C. L., et al. (2004), The ocean sink for anthropogenic CO_2, *Science*, *305*, 367–371.

Schuster, U., and A. J. Watson (2007), A variable and decreasing sink for atmospheric CO_2 in the North Atlantic, *J. Geophys. Res.*, *112*, C11006, doi:10.1029/2006JC003941.

Takahashi, T., R. A. Feely, R. F. Weiss, R. H. Wanninkhof, D. W. Chipman, and S. C. Sutherland (1997), Global air-sea flux of CO_2: An estimate based on measurements of sea-air pCO_2 difference, *Proc. Natl. Acad. Sci.*, *94*, 8292–8299.

Takahashi, T., et al. (2002), Global sea air CO_2 flux based on climatological surface ocean pCO_2, and seasonal biological and temperature effects, *Deep Sea Res. II*, *49*, 1601–1622.

Wanninkhof, R. (1992), Relationship between windspeed and gas exchange over the ocean, *J. Geophys. Res.*, *97*(C5), 7373–7382.

Watson, A. J., C. Robinson, J. E. Robinson, P. J. le B. Williams, and M. J. R. Fasham (1991), Spatial variability in the sink for atmospheric carbon dioxide in the North Atlantic, *Nature*, *350*, 50–53.

T. Friedrich, International Pacific Research Center, SOEST, University of Hawai'i at Manoa, East-West Road 1680, Post Building 412F, Honolulu, HI 96822, USA. (tobiasf@hawaii.edu)

A. Oschlies, Leibniz-Institut für Meereswissenschaften an der Universität Kiel (IfM-GEOMAR), Düsternbrooker Weg 20, D-24105 Kiel, Germany. (aoschlies@ifm-geomar.de)